Research article

Motion planning for omni-directional mobile robots based on anisotropy and artificial potential field method

Chuntao Leng
School of Mechanical Engineering, Shanghai Jiao Tong University, Shanghai, China, and

Qixin Cao
Research Institute of Robotics, School of Mechanical Engineering, Shanghai Jiao Tong University, Shanghai, China

Abstract

Purpose – The purpose of this paper is to propose a suitable motion planning for omni-directional mobile robots (OMRs) by taking into account the motion characteristics.

Design/methodology/approach – Based on the kinematic and dynamic constraints, the maximum velocity, motion stability and energy consumption of the OMR moving in different directions are analysed, and the anisotropy of the OMR is presented. In order to obtain the optimal motion, the path that the robot can take in order to avoid the obstacle safely and reach the goal in a shorter path is deduced. According to the new concept of anisotropic function, the motion direction derived from traditional artificial potential field (tAPF) is regulated.

Findings – A combination of the anisotropic function and tAPF method produces high-speed, highly stable and efficient motion when compared to the tAPF. Simulations and experiments have proven the validity and effectiveness of this method.

Research limitations/implications – The practical factors, such as the effect of wear on the omni-directional wheels, are not considered. Typical problems of APF, e.g. local minima, are not addressed here. In our future research, we will deal with these issues.

Practical implications – The proposed motion planning is applicable for any kind of OMRs, both three- and four-wheeled OMRs, which can fully exhibit the advantages of OMRs.

Originality/value – The new concept of an anisotropic function is proposed to indicate the quality of motion in different directions. Different motion effects can be obtained in the same direction with different weights denoted by the anisotropic function, i.e. different trade-offs can be achieved by varying the weights.

Keywords Robotics, Motion, Control technology

Paper type Research paper

1. Introduction

Motion planning is an important branch of mobile robot research, and collision-free path planning also plays an important role for omni-directional mobile robot (OMR) study. Different from traditional mobile robots, OMRs can achieve translation along any arbitrary direction without rotation, which results in their agile performance (Pin and Killough, 1994). The maximum velocity and acceleration (Wu *et al.*, 2006), motion stability and motion efficacy are different while it moves in a different direction, this is called anisotropy. Especially, owing to the different applications (Tlale, 2006; Chatzakos *et al.*, 2006), the arrangements of the omni-directional wheels are not generally symmetrical, which makes the anisotropy much more distinct. Accordingly, the motion planning of OMRs along different directions result in different trajectories and motion efficacy, and the research of collision-free path planning for OMRs are crucial.

Owing to the anisotropy of motion characteristics, the former motion planning applicable for traditional mobile robots is not suitable for OMRs. Felipe and Miguel (2006) analysed and compared three path planning methods for omni-directional robots, which are based on the Bug algorithm, the potential fields algorithm and the A* algorithm. Suzuki and Shin (2005) used the descendent gradient of a navigation function to find a shorter and safer path for OMRs. To achieve a high-speed navigation, Brock and Khatib (1999) considered the agile performance of OMRs, and proposed a global dynamic window approach. But all of them considered the OMR as an isotropic problem and therefore the potential of OMRs were not fully exhibited.

There are also many papers on the trajectory control of OMRs, which have taken into consideration, the motion

The current issue and full text archive of this journal is available at **www.emeraldinsight.com/0143-991X.htm**

Industrial Robot: An International Journal
36/5 (2009) 477–488

[DOI 10.1108/01439910910980204]

This paper is supported by the National High Technology Research and Development Program of China (863 Program), 2007AA041602-1.

Industrial Robot: An International Journal
Volume 36 · Number 5 · 2009 · 477–488

characteristics. Balkcom *et al.* (2006) considered a kinematic model of the vehicle and placed independent bounds on the speeds of the wheels, and derived the fastest trajectories between configurations. Wang *et al.* (2007) solved the time-optimal control problem as a constrained nonlinear programming problem according to the kinematic model. Kalmar-Nagy *et al.* (2004) made use of the characteristics of OMRs to simplify the control problem, and presented an algorithm for a near-optimal dynamic trajectory generation with low computational cost. Koh and Cho (1999) considered the dynamic constraints for a smooth path tracking to avoid wheel slippage and mechanical damage based on "bang-bang" control.

Wu *et al.* (2006) proposed the novel concepts of velocity and acceleration cones for determining the kinematic and dynamic constraints, and studied the motion planning of OMRs without obstacles. Wu (2004) presented the research about motion planning of OMRs in his PhD dissertation. Using the ability of translation along arbitrary directions, a coordinating velocity in the vertical direction of motion was introduced to accommodate maneuvers for a safe route.

Most work on motion planning for OMRs focused on the time optimality, and there are few studies on the stability and the motion efficacy by analysis of kinematic and dynamic characteristics. For optimal motion planning, making a proper trade-off between time optimality, stability and efficacy optimality is very important.

Owing to its simplicity and mathematical elegance, artificial potential field (APF) is widely used for collision-free path planning. Originally, the APF developed by Khatib (1986) was used in a stationary environment. However, because environments are dynamic in most real-world implementations, APF has been improved to suit the extensive environments in the past decade. For examples, Zheng and Zhao (2006) proposed an evolutional APF for dynamic environments, and Luh and Liu (2007) proposed a potential field immune network. Also, an artificial coordinating field was introduced to APF by Jing *et al.* (2004), i.e. a coordinating force was used for coordinating the APF. For an optimal control system, Shimoda *et al.* (2005) considered the dynamic constraints and dynamic environments into APF.

Although, APF has been studied for OMRs, for example, Ge and Cui (2002) proposed a new APF method in dynamic environments where the goal and the objects are moving, and made a motion planning for OMR with the method. Samani *et al.* (2004) described an omni-directional soccer robot system, in which APF was used for the trajectory planning. There have not been any APF that takes into consideration the characteristics of OMRs. And the anisotropy of OMRs was also not taken into account. The motion planning of OMR along different directions results in different trajectories and motion efficacy. To achieve a high-speed, highly stable and highly efficient navigation, it is necessary to improve the APF for the application to OMRs.

Owing to the agile performance and anisotropy, considering the effects of the dynamic environment, based on traditional APF (tAPF), the study on an improved motion planning algorithm which will result in a short-trajectory, high-speed, highly stable, highly efficient, collision-free path is the main objective of this paper. Especially, the OMR with different wheel arrangements, such as three- and four-wheeled OMRs, are analysed for the universality of the proposed motion planning method.

The concept of an anisotropic function based on the analysis of kinematics and dynamics of OMRs is proposed, which synthesizes the velocity, motion stability and motion efficacy. Especially, the driving torque acting on each wheel is discussed for the motion stability. By regulating the weights of the anisotropic function, we can obtain a proper trade-off between time optimality, stability and efficacy optimality. And the "variable motion direction area (VMDA)" for a collision-free path and shorter path are defined according to the information of the robot, obstacles and goal. The motion direction worked out by tAPF was coordinated by an anisotropic function for the optimal motion. Finally, an improved motion planning method which can fully exhibit the advantages of OMRs is proposed. With the ability to translate along any arbitrary direction, the trajectory in this research is composed of a piecewise translation motion, i.e. the orientation of the robot will not change.

Both the three- and four-wheeled OMR are discussed in this paper. Simulations and experiments were carried out on the OMRs developed in our laboratory, such as the home care robot and the soccer robot, and the results were promising.

The present paper is organized as follows: Section 2 presents the modelling of an anisotropic function; Section 3 describes the VMDA; in Section 4, an improved APF (iAPF) is proposed based on the anisotropic function and the APF method; Section 5 illustrates the effectiveness of the improved motion planning by performing simulations and experiments; finally, conclusions are drawn in Section 6.

2. Anisotropy analysis for OMRs

2.1 Maximum velocity analysis

There are many kinds of omni-directional wheels (Ferriere *et al.*, 1996). In this paper, we discuss the Mecanum wheel which is shown in Figure 1. The OMR can consist of three or four omni-directional wheels, such as a three- and four-wheeled OMR shown in Figure 2(a) and (b). With different arrangements of the wheels, the performance of OMR is distinct. In the following section, the maximum velocity of OMR will be deduced.

First, we will build the kinematic model for analysing the velocity characteristics of the OMR (Angeles, 2003). According to the velocity relationship of the driving roller and the passive roller as shown in Figure 1, the velocity of the driving roller centre $\boldsymbol{o}_i$ can be determined by equation (1). Meanwhile the velocity $\boldsymbol{o}_i$ also can be denoted by the velocity of robot centre ($\boldsymbol{c}$) and angular velocity $\boldsymbol{\omega}$, which is shown in equation (2). Owing to the passive rollers not being driven by a motor, the angular velocity of the passive roller $\dot{\boldsymbol{\phi}}_i$ is irrelevant to our study, and can be eliminated during kinematic analysis. Dot-multiplied by the axle vector $\boldsymbol{E}_i$ on both sides of equations (1) and (2), we can derive equation (3) as a general kinematic equation for the OMR, where $\boldsymbol{d}_i$ denotes the vector from the point of robot centre C to the point of driving roller centre $\boldsymbol{o}_i$, R and r are the radiuses of the driving roller and passive roller, respectively, $\dot{\boldsymbol{\theta}}_i$ is the regular velocity of the driving roller, and the vector $\boldsymbol{U}_i$ and $\boldsymbol{Z}_i$ are defined as in Figure 1:

$$\dot{\boldsymbol{o}}_i = -R\dot{\boldsymbol{\theta}}_i\boldsymbol{U}_i - r\dot{\boldsymbol{\phi}}_i\boldsymbol{Z}_i \tag{1}$$

$$\dot{\boldsymbol{o}}_i = \dot{\boldsymbol{c}} + \dot{\boldsymbol{\omega}}\xi d_i \quad \text{where } \xi \equiv \begin{bmatrix} 0 & -1 \\ 1 & 0 \end{bmatrix} \tag{2}$$

$$-R\dot{\boldsymbol{\theta}}_i = \boldsymbol{E}_i\xi\boldsymbol{d}_i, \boldsymbol{E}_i]\mathbf{t}, \quad i = 1, 2, \ldots, n \quad \text{where } \mathbf{t} \equiv \begin{bmatrix} \boldsymbol{\omega} \\ \dot{\boldsymbol{c}} \end{bmatrix} \tag{3}$$

Figure 1 Omni-directional wheel

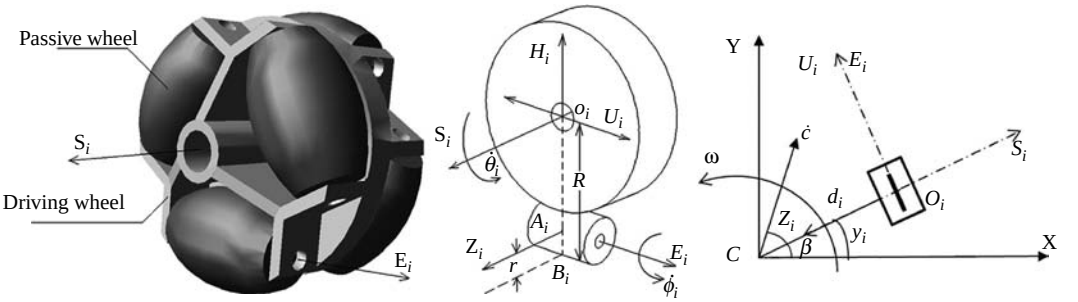

Figure 2 Omni-directional mobile robot

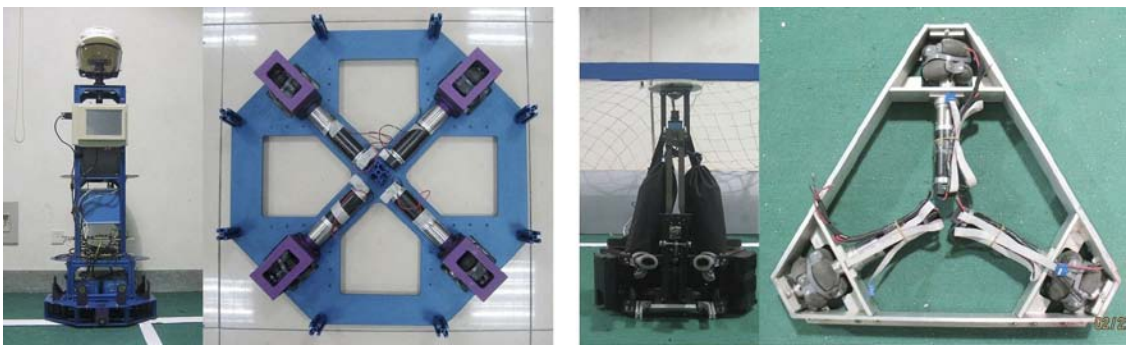

(a) Four-wheeled OMR

(b) Three-wheeled OMR

Taking into consideration, the special mechanism of the omni-directional wheel, analysing the maximal magnitude of velocity is important for designing a robot with good performance. According to the maximum velocity that three- and four-wheeled OMRs can achieve, it can be used consequently to determine the arrangement of the omni-directional wheels.

For simplification, we transform the kinematic equation (3) into equation (4), where β denotes the angle between vector $\boldsymbol{d}_i$ and x-axis, γ_i denotes the angle between $\boldsymbol{S}_i$ and X-axis (Figure 1), and the subscript i is the sequence number of the wheel. With the ability of translate along any arbitrary direction, the trajectory can be composed of a piecewise translation motion, therefore we only take into account the translational velocity, i.e. $\boldsymbol{\omega} = \mathbf{0}$:

$$R\dot{\boldsymbol{\theta}}_i = \dot{\boldsymbol{c}}\sin(\beta - \gamma_i) \quad i = 1, 2, \ldots, n \tag{4}$$

The derivation details for maximum velocity are discussed in the former literature (Leng and Cao, 2006). To work out the maximum velocity in some direction (β) of the robots, the problem can be described as determining the maximal magnitude of $\dot{\boldsymbol{c}}$ when β is equal to a certain value. Let $M_i = \sin[\theta - 2(i-1)\pi/K]$, and the maximum magnitude of $|M_i|$ as $|M_i|_{\max}$, where K is the number of the omni-directional wheels. Then, the maximum magnitude of velocity of the robot in the direction β can be noted as $V_{c\beta}$ ($V_{c\beta} = 1/|M_i|_{\max}$, supposing that the maximal velocity of each wheel is 1 m/s). Finally, we can obtain the maximum velocity curves shown in Figure 3(a) and (b) for four- and three-wheeled OMR, respectively. (Owing to the symmetry, only the case of 0-180° is discussed in this work.)

From Figure 3, we can conclude that, the maximum velocity of the four-wheeled OMR is higher than that of the three-wheeled OMR. According to Figure 3, for high-speed motion planning, we should coordinate the robot to move between the range of 0, 90 or 180° for four-wheeled OMR and 0, 60, 120° or 180° for three-wheeled OMR.

2.2 Dynamics and motion stability analysis

Small-sized mobile platforms and high centre of gravity are particularly prone to "tip-overs", which is a necessary pre-requisite to solve for applications in homes or offices. Therefore, it is important to achieve a stable motion for OMRs, such as the robot shown in Figure 2(a). In this section, we focus on the study of motion stability.

The driving torque acting on each wheel of OMRs is much bigger than traditional mobile robots. Because the power for DC motors is supplied by a portable battery, when the power decreases with respect to time during operation, some motors cannot supply enough driving torque for a coordinated motion, which will result in the slip phenomenon and unstable motion. As anisotropic characteristics, the driving torque acting on each wheel while moving in some direction is distinct. For stable motion, it is better to let the robot move in the direction in which the driving torque is not large.

Also, the maximum acceleration in different directions are different, to avoid slippage, and it is necessary to work out the maximum acceleration while the robot moves along some direction. We also need to avoid exceeding the maximum acceleration to prevent "skipping". By performing practical experiments, we can obtain the conclusion as follows: if the motion can achieve a much higher maximum acceleration along some direction, then it can achieve much less slip and stable acceleration in this direction; however, more slippage occurs.

In this paper, only the four-wheeled OMR will be analysed in the following sections. The analysis for the three-wheeled

Figure 3 Maximum velocity curve

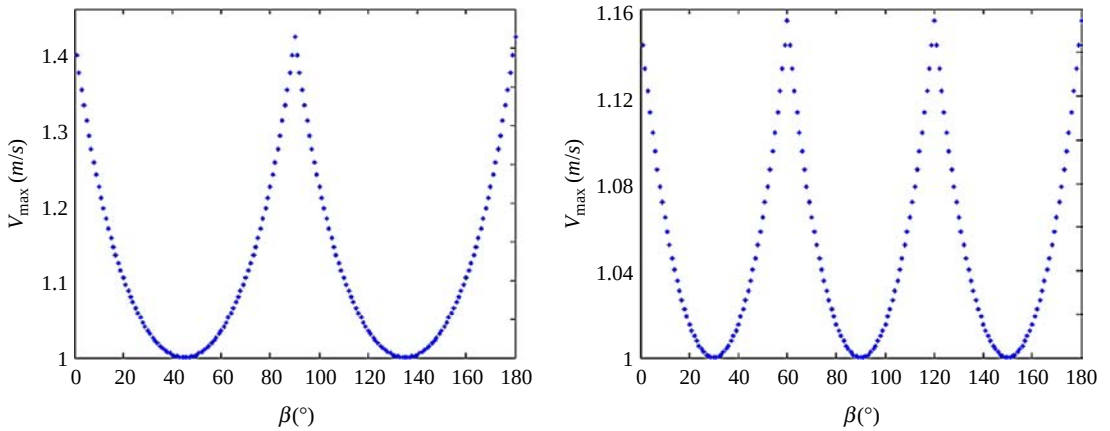

(a) Maximum velocity of four-wheeled OMR

(b) Maximum velocity of three-wheeled OMR

OMR is the same as the deduction derived for the four-wheeled OMR.

2.2.1 Driving torque analysis

Based on the theory of vehicle dynamics (Yu, 1990), while the OMR accelerates, the tangential force caused by the contact deformation between the driving wheel and the ground is the traction of the mobile robot. Rolling resistance couple resulting from the deformation of the wheel counteracts the rotation of the driving wheel, and the passive wheel is also subject to effects of the tangential force and resistance couple. The unitary force diagram and the force during the accelerating period of OMR are shown in Figure 4.

Parameters are defined as follows: $\boldsymbol{P}_{\mathrm{d}}$ and $\boldsymbol{P}_{\mathrm{p}}$ are the gravitational loads acting on driving wheel and passive wheel, respectively. $\boldsymbol{N}_{\mathrm{d}}$ and $\boldsymbol{N}_{\mathrm{p}}$ are the normal counter-force acting on the driving wheel and passive wheel by the ground. $\boldsymbol{f}_{\mathrm{d}i}$ and $\boldsymbol{f}_{\mathrm{p}i}$ are the tangential counter-force acting on the driving wheel and passive wheel by the ground at the point of contact, and the subscript i is the sequence number of the wheel. $\boldsymbol{F}'$ and $\boldsymbol{Q}_{\mathrm{p}}$ are the component of forces acting on the driving wheel and passive wheel by the driving axis and passive axis, respectively, and they are parallel to the ground. $\boldsymbol{M}_{\mathrm{Pd}}$ and $\boldsymbol{M}_{\mathrm{Pp}}$ are the rolling resistance moments acting on the driving wheel and passive wheel, and they are almost invariable if the robot load is fixed. $\boldsymbol{\varepsilon}_{\mathrm{d}i}$ and $\boldsymbol{\varepsilon}_{\mathrm{p}i}$ are the angular accelerations of the driving wheel and passive wheel, and $\boldsymbol{a}_{\mathrm{d}i}$ and $\boldsymbol{a}_{\mathrm{p}i}$ are the components of acceleration of the driving wheel centre and passive wheel centre, respectively, and they are parallel to the ground. $\mathcal{J}_{\mathrm{d}}$ and $\mathcal{J}_{\mathrm{p}}$ are the moments of inertia of the driving wheel and passive wheel, respectively. $\boldsymbol{T}_i$ is the driving torque of the motor.

Figure 4 Force analysis

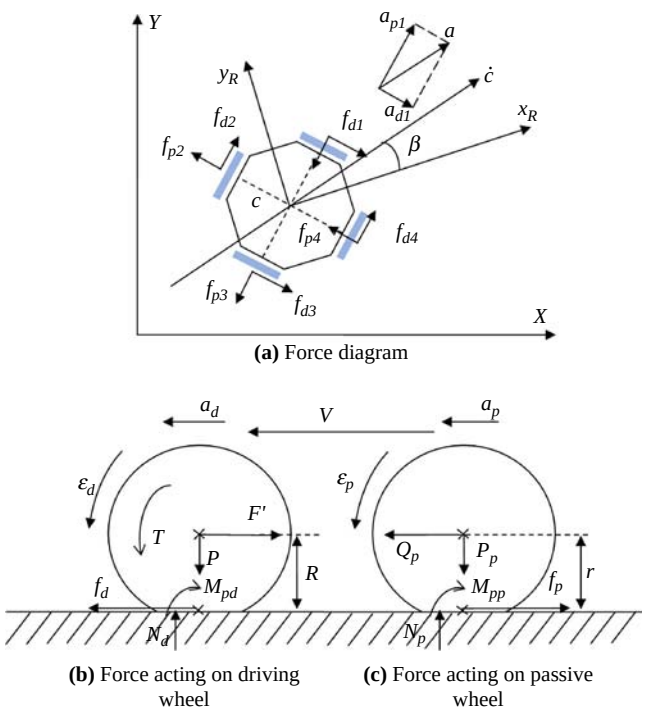

(a) Force diagram

(b) Force acting on driving wheel

(c) Force acting on passive wheel

According to the force diagram (Figure 4), the dynamic model of driving wheel and passive wheel (Yu, 1990) are defined by equations (5) and (6). Where m_{d} is the mass of driving wheel, and m_{p} is the mass of passive wheel:

$$m_{\mathrm{d}}\boldsymbol{a}_{\mathrm{d}i} = \boldsymbol{f}_{\mathrm{d}i} - \boldsymbol{F}' \qquad \mathcal{J}_{\mathrm{d}}\boldsymbol{\varepsilon}_{\mathrm{d}i} = \boldsymbol{T}_i - \boldsymbol{f}_{\mathrm{d}i}R - \boldsymbol{M}_{P_{\mathrm{d}}} \tag{5}$$

$$\begin{aligned} m_{\mathrm{p}}\boldsymbol{a}_{\mathrm{p}i} &= \boldsymbol{Q}_{\mathrm{p}} - \boldsymbol{f}_{\mathrm{p}i} \\ \mathcal{J}_{\mathrm{p}}\boldsymbol{\varepsilon}_{\mathrm{p}i} &= \boldsymbol{f}_{\mathrm{p}i}r - \boldsymbol{M}_{P_{\mathrm{p}}} \end{aligned} \tag{6}$$

Owing to symmetry of the structure, only the case of $0 \leq \beta \leq 180°$ is discussed in this work, β is the motion direction in the local coordinate system $\{c, x_R, y_R\}$. For simplification, it is assumed that the robot moves in direction β without rotation. To analyse the specifics of the driving torque, the driving torque acting on each wheel when the robot moves in different directions will be analysed in Section 2.2.2. In Section 2.2.2, we will only analyse the case where the direction of acceleration β is subjected to $\beta < 45°$, and the force diagram is shown in detail in Figure 4(a).

As shown in Figure 4(a), in the local coordinate system $\{c, x_R, y_R\}$, suppose that the robot moves in the direction of β only with the translational motion, and the acceleration is a. Then according to the Newton's second law, we can obtain the equation (7), where $\alpha = 45°$. Owing to the symmetry of the omni-directional wheel arrangement, we know $f_{\mathrm{d}1} = f_{\mathrm{d}3}$,

$f_{d2} = f_{d4}$, $f_{p1} = f_{p3}$, $f_{p2} = f_{p4}$, and because there is only translation without rotation, $f_{d1} + f_{d3} = f_{d3} + f_{d4}$:

$$\begin{cases} 2f_{d2}\cos(\alpha-\beta)+2f_{d1}\cos(\alpha+\beta)-2f_{p2}\cos(\alpha+\beta)-2f_{p1} \\ \quad \cos(\alpha-\beta)=ma \\ 2f_{d2}\sin(\alpha-\beta)+2f_{p2}\sin(\alpha+\beta)=2f_{d1}\sin(\alpha+\beta)+2f_{p1} \\ \quad \sin(\alpha-\beta) \end{cases} \quad (7)$$

According to equation (6), the tangential counterforce acting on the passive wheel by the ground at the point of contact can be obtained by equation (8):

$$f_{pi} = \frac{\mathcal{J}_{pi} a_{pi}}{r^2} + \frac{M_{\boldsymbol{P}_p}}{r} \quad i = 1,2,3. \quad (8)$$

In Figure 4(a), the relation between a_{pi} and a is shown in equation (9):

$$\begin{aligned} a_{p1} &= a\cdot\cos(\beta) \\ a_{p2} &= a\cdot\cos(90-\alpha+\beta) = a\cdot\sin(\alpha-\beta) \\ a_{p3} &= a\cdot\cos(90-\alpha-\beta) = a\cdot\sin(\alpha+\beta) \end{aligned} \quad (9)$$

Substituting the equations (7)-(9) into equation (5), we can obtain the driving torque acting on driving wheel $\boldsymbol{T}_i$. With the same deduction, we can obtain $\boldsymbol{T}_i$ while β varied in (0, 180°). The results are shown in Figure 5. According to the curve, the driving torque in the direction vector 45 and 135° is maximum, therefore, we should avoid the motion in this direction to achieve a stable motion plan.

2.2.2 Maximum acceleration analysis

According to the Newton's Second law, we can obtain the equation (10) along the accelerating direction of the passive wheel 1, and the formulae for the other wheels are the same:

$$2\boldsymbol{f}_{d2} - 2\boldsymbol{f}_{p1} = ma\cos(\alpha-\beta) = ma_{p1} \quad \text{where } \alpha = 45° \quad (10)$$

where m is the mass of the robot.

During the acceleration, $\mathcal{J}_p \cdot \boldsymbol{\varepsilon}_p \ll \boldsymbol{M}_{\boldsymbol{P}_p}$, the tangential force $\boldsymbol{f}_p \approx \boldsymbol{M}_{\boldsymbol{P}_p}/r$ can be deduced by equation (6). And the driving force is offered by the adhesive force, so the maximum value is $\boldsymbol{f}_{dmax} = \boldsymbol{u}_h \cdot \boldsymbol{P}$, where u_h is the adhesion parameter, $\boldsymbol{P}$ is the normal pressure acting on ground by the wheel. Therefore, when $\boldsymbol{f}_{d2} \to \boldsymbol{f}_{d2max}$, the acceleration $\boldsymbol{a}$ will reach the maximum according to the equation (10). In the same way, the maximum acceleration in other direction can be worked out. Finally, the maximum acceleration of the four-wheeled OMR is shown in Figure 6.

The maximum acceleration in the direction vector 45° is minimum according to Figure 6, therefore, we should avoid the motion in this direction to achieve a high-speed and highly stable motion plan.

2.3 Motion consumption analysis

For an autonomous mobile robot, the power is usually supplied by a battery. And in our case where the omni-directional wheel is used for the OMR, the load condition is distinct when the robot moves along different directions, which results in differences in the motion efficacy. The motion efficacy is an important control indicator for the motion planning of an OMR.

To compare the motion efficacy, we work out the motor consumption when the robot moves in different directions under the same conditions. The motor consumption is determined by motor torque T in equation (11) here for simplification, where W_a and W_v are the energy consumption in accelerated motion and uniform motion, respectively, T_a and T_v are the motor torques in accelerated motion and uniform motion, respectively, t_a and t_v are the time consumption in accelerated motion and uniform motion, respectively, ε_e is the angular acceleration, and ω_e is the angular velocity in uniform motion:

$$\begin{cases} W_a = \frac{1}{2} T_a \varepsilon_e t_a & \text{accelerated motion} \\ W_v = T_v \omega_e t_v & \text{uniform motion} \end{cases} \quad (11)$$

According to the analysis in Section 2.2, the driving torque T_a and T_v can be determined. When analysing the uniform motion of the OMR, the forces are the same as shown in Figure 4, and we set $\boldsymbol{a} = 0$ in equation (7). To compare the motion efficacy while moving along different directions, we determine the motor consumption during accelerated motion and uniform motion along different directions under the same conditions, i.e. the initial velocity is 0, acceleration is $\boldsymbol{a}$,

Figure 5 Driving torque cure

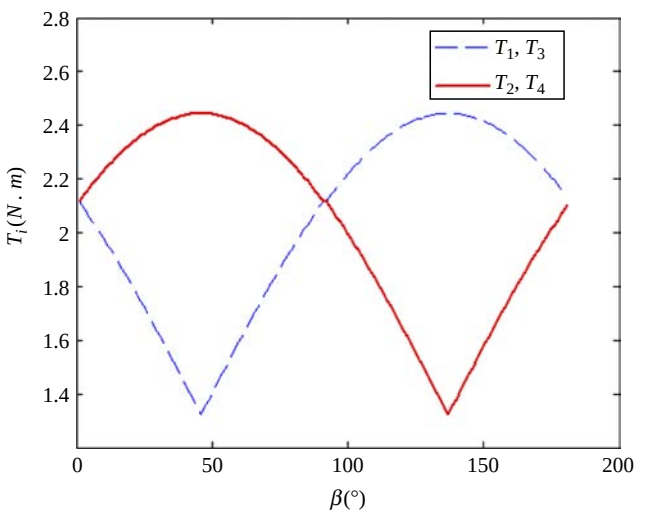

Figure 6 Maximum acceleration in different directions

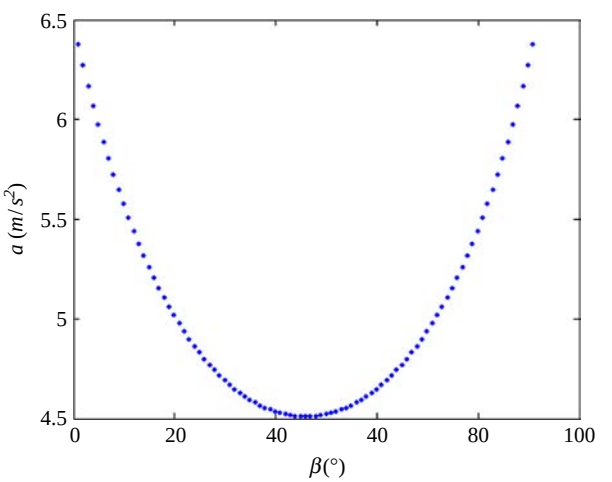

uniform velocity is v, and the moving time is t. Finally, we obtain the consumption is W, and according to the analysis above, we obtained the result for the four-wheeled OMR as shown in Figure 7.

In Figure 7, it can be seen that motion efficacy is highest while the robot moves in the direction of around 45°. To economize the limited power, it is necessary to make the robot move along the direction of highest efficacy for the motion planning.

2.4 Anisotropic function

For the motion planning, the velocity, the motion stability and the motion efficacy are important indicators. With the special mechanism of the omni-directional wheels, the anisotropic characteristics are distinct. As the maximum velocity, the motion stability and the motion efficacy analysed above, the motion effects along different directions are distinct.

Synthesizing the anisotropic characteristics of driving torque ($\tau(\beta)$) and maximum acceleration ($A(\beta)$), the anisotropic characteristics of motion stability ($S(\beta)$) can be deduced. First, we take the driving torque curve which achieved the maximum as the influential torque, such as T_2 and T_4 when $0° < \beta < 90°$, T_1 and T_3 when $90° < \beta < 180°$ in Figure 5. After obtaining the reciprocal of the influential torque, we convert it into [0, 1], and also convert maximum acceleration (Figure 6) into [0, 1]. Adding the two items with the same weight, i.e. $S(\beta) = k_\tau \tau(\beta) + k_A A(\beta)$, where $k_\tau = k_A = 0.5$, it results in the anisotropic characteristics of motion stability.

Then we convert the value of maximum velocity (Figure 3) and energy consumption (Figure 7) into [0, 1], and especially convert the energy consumption curve into the motion efficacy curve by getting the reciprocal of the energy consumption value. Then we can deduce $V(\beta)$ and $E(\beta)$ as the anisotropic characteristics of velocity and efficacy, respectively. Finally, we introduce the anisotropic function as shown in equation (12), where k_1, k_2 and k_3 are functional weights:

$$\begin{aligned} G(\beta) &= k_1 V(\beta) + k_2 S(\beta) + k_3 E(\beta) \\ &= k_1 V(\beta) + k_2 (k_\tau \tau(\beta) + k_A A(\beta)) + k_3 E(\beta) \end{aligned} \quad (12)$$

Figure 7 Energy consumption in different directions

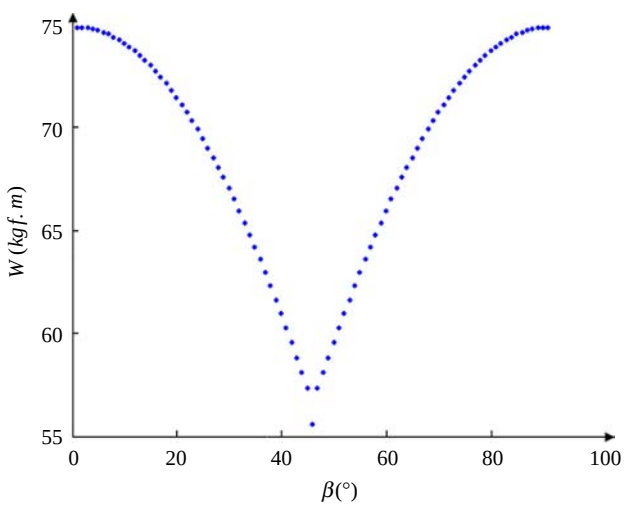

The anisotropic function value is an indicator to weigh the motion effects in the corresponding direction, where the higher the value, the better the motion effects in this direction will be. There will be different motion effects in the same direction with different weights denoted by the anisotropic function, i.e. different trade-offs can be achieved by varying the weights. For the home care robot, it is important to highlight the impact of motion stability, so we can increase the functional weight, for example, we take $k_1 = 20$ per cent, $k_2 = 60$ per cent and $k_3 = 20$ per cent. Therefore, the direction corresponding to the maximum value of the anisotropic function is the optimum motion direction for the expected motion effect. Based on the motion direction worked out by tAPF, according to the anisotropic function value of each direction, we regulate the motion direction to achieve the optimal motion planning. According to the anisotropic function and the analysis above, we can get the anisotropic function curve shown in Figure 8, where $k_1 + k_2 + k_3 = 1$.

With the same analysis, we also can obtain the anisotropic function of the three-wheeled OMR.

3. Variable motion direction area

According to the anisotropic function of OMRs, we can achieve optimal motion by regulating the motion direction worked out by tAPF. Whereas, to achieve collision-free motion planning, not only the characteristics of the OMR be considered, but we also need to take into account the information of obstacles and goal. Because the motion along the optimum direction may not result in the optimum path plan, the VMDA that the robot can avoid collision must be determined. Meanwhile, the path length will directly influence the speed and efficacy of motion planning, so the VMDA for the shorter path must also be determined.

3.1 VMDA for collision-free path

While regulating the motion direction according to the anisotropic function, we did not consider the influence of the obstacles; therefore, it is possible to achieve high-speed motion planning without obstacle avoidance.

In order not to take into account the influence of avoiding obstacles for high-speed motion planning, when the threat of obstacles is big, the range for robot to regulate the motion direction will be small. The relative position and velocity are

Figure 8 Anisotropic function curve

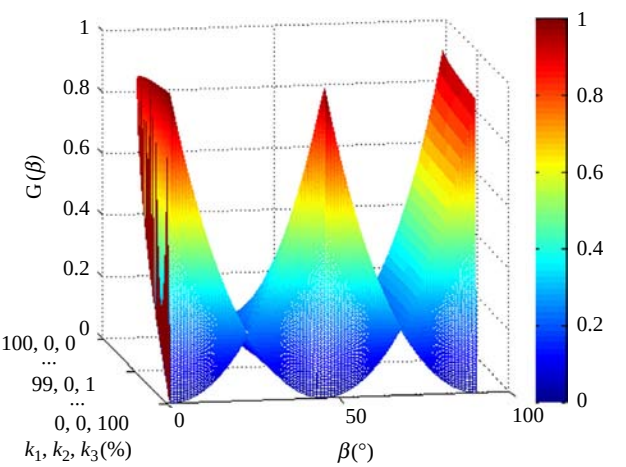

the key factors that should be considered. Therefore, at the relative velocity $\boldsymbol{v}_{or}$, the time needed when the robot collides with obstacles and the time needed when obstacle moves towards the direction of the robot motion, are noted as an impact factor to define the variable angle. Therefore, it can be modelled as shown in equation (13). Where β_o is the variable motion direction range with obstacle avoidance, k_a and k_b are the coordinating parameters, D_{or} is the relative distance between robot and obstacle, δ is the angle between $\boldsymbol{v}_{or}$ and OR, γ is the angle between the velocity of the robot ($\boldsymbol{v}_r$) and OR, which are shown in detail in Figure 9:

$$\beta_o = \left(\frac{k_a D_{or}}{v_{or}\cos\delta}\right) + \left(\frac{k_b D_{or}.\gamma}{v_{or}\sin\delta}\right) \tag{13}$$

Varying the direction in the range of β_o calculated by equation (13) will not influence the avoidance effect, which is called the VMDA for collision-free path. When there is more than one obstacle, taking the minimum of the VMDA as the final safe area is the area we can vary the motion direction.

3.2 VMDA for the shorter path

The maximum velocity in each direction is shown in polar coordinates, and the rhombus ($V_0V_{90}V_{180}V_{270}$) is the maximum velocity curve from 0° to 360° (Figure 10).

Figure 9 Effect on APF caused by relative movement

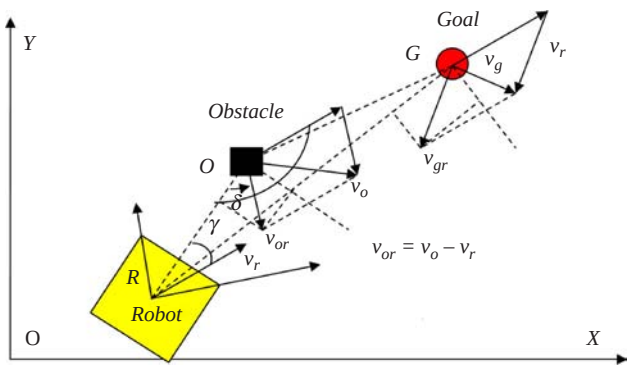

Figure 10 VMDA for a shorter path

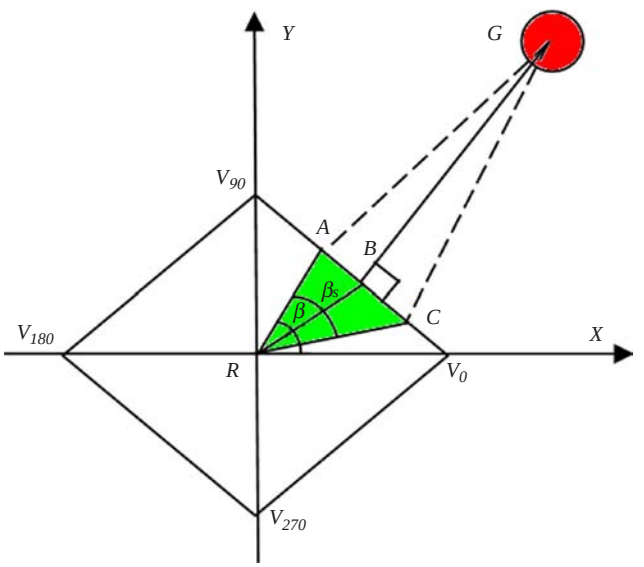

For example, the length RA is the maximum velocity in the direction of β. For high-speed motion planning, the length of the path is the important indicator. Accordingly, to achieve optimal motion planning, it is necessary to ensure that the path varied by the anisotropic function is shorter than the one resulting from tAPF. As shown in Figure 10, RA is the motion direction resulting from tAPF, G is the goal, and GB is the vertical of V_0V_{90}, therefore, when the robot moves along RB, the distance between the robot and the goal will be the minimum. GC is the symmetrical line of GA with regard to GB, it is obvious that if the robot moves in the angle range of β_s, the distance between robot and goal will be nearer than the one in the direction of β, i.e. the motion along the direction in the shaded region (β_s) will achieve a shorter path, and β_s is called the VMDA for a shorter path.

4. A new motion planning method

4.1 Traditional APF

The basic principle of APF is to construct attractive potential fields around the goal to attract the robot and to construct repulsive potential fields around the obstacles to force the robot away from it. There has been a lot of classical research on APF, with different kinds of attractive and repulsive potential fields that has been introduced. In our study, we take the APF proposed by Khatib (1986) as reference to derive the suitable motion planning for an OMR, and the artificial potential field is defined in equation (14):

$$\begin{aligned} \boldsymbol{F}_{att} &= n_1 D_{rg}\boldsymbol{n}_{RG} \\ \boldsymbol{F}_{rep} &= -n_2\left(\tfrac{1}{D_{ro}} - \tfrac{1}{D_0}\right)\tfrac{1}{D_{ro}}\,\boldsymbol{n}_{RO} \\ \boldsymbol{F} &= \boldsymbol{F}_{att} + \boldsymbol{F}_{rep} \end{aligned} \tag{14}$$

where $\boldsymbol{F}_{att}$ and $\boldsymbol{F}_{rep}$ are attraction and repulsion, respectively, $\boldsymbol{F}$ is the resultant force of attraction and repulsion, i.e. the force used to drive the robot. D_{rg} and D_{ro} are the relative distance from the robot to the goal and obstacles, respectively,. $\boldsymbol{n}_{RG}$ and $\boldsymbol{n}_{RO}$ are unit vectors from the robot to the goal and obstacles, respectively. n_1 and n_2 are the coordinating parameters. D_0 represents the limited distance of the potential field influence.

4.2 Improved APF method based on anisotropic function

APF is widely used in the motion planning for mobile robots, but the application of tAPF to OMR, cannot fully exhibit the motion advantage of OMR. Therefore, it is important to consider the characteristics of OMRs to propose a suitable motion planning. In this paper, we use the anisotropic function $G(\beta)$ to improve the tAPF. In this algorithm, the optimal motion direction we need is worked out in the VMDA determined according to the collision-free and shorter path principle.

In our approach, we use the total potential field force as steering control (Ge and Cui, 2002) to exhibit the potential of an OMR, i.e. the motion direction is determined by the anisotropic function and the VMDA.

Using the tAPF, the motion direction resulted from the total potential field force is deduced, which is denoted by the bold broken line shown in Figure 11. The VMDA for collision-free is noted as β_o, and the VMDA for shorter path is noted as β_s. Then the final VMDA is their overlapping region. According to the anisotropic function $G(\beta)$, the optimum

Figure 11 Motion direction resulting from iAPF

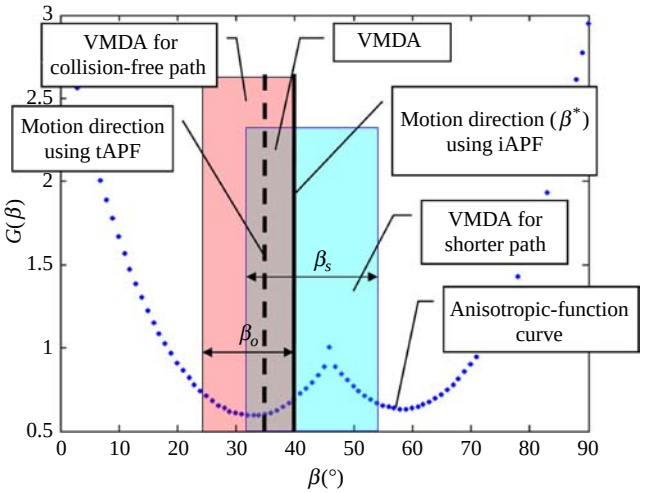

motion direction β^* can be derived from equation (15), and it is denoted by the bold real line in Figure 11. Finally, the motion direction β^* is the very motion direction for the improved motion planning:

$$\beta^* = \arg\max G(\beta) \quad \beta \in \beta_o \cap \beta_s \tag{15}$$

After determining the motion direction, we should determine the motion velocity. Here, the motion velocity is determined by the distance between robot and obstacles. When the robot is far away from obstacles, the velocity will reach the maximum. When the distance is less than some threshold (D_0), the velocity will be reduced. At this moment, the velocity will be proportional to the relative distance between the robot and obstacle as it is no longer affected by the functional weight k_1 of the anisotropic function.

From the analysis, we mentioned above, we can build the following velocity model in equation (16), where, v_{max} is the maximum velocity value in the motion direction. K_0 is the coordinating parameter:

$$v = \begin{cases} v_{max} & D_{ro} \geq D_0 \\ k_0 \frac{D_{ro}}{D_0} v_{max} & D_{ro} < D_0 \end{cases} \tag{16}$$

5. Simulation and experiments

5.1 Simulation studies

In order to validate the generalization of the iAPF, we do simulation studies on both three- and four-wheeled OMR. To validate the effectiveness of the motion planning mentioned in this study, we carry out a simulation in Matlab to analyse and compare tAPF to our iAPF.

The motion stability item in the anisotropic function is to weigh the stability in different directions, but the simulation in this study do not consider the occurrence of skids, therefore, only the high-speed and highly efficient cases can be validated in the simulation, and the stability anisotropy will be validated in the practical experiments. Therefore, in the simulations, we compare the time and the energy expended at the same initial condition while performing a similar task. In order to fully evaluate the improved motion planning model, the path length and the average velocity are also compared.

The motion stability item also includes the acceleration which influences the time consumption, so we vary the value of k_1:k_2:k_3 to determine the optimal functional weights. The main part of the initial setup for the simulation is shown in Table I, and all of the values are determined according to the real robot, where P_4(N) is the weight of the four-wheeled OMR, and P_3(N) is the weight of the three-wheeled OMR. Primarily, the coordinating parameters are experiential, and we can obtain the optimum by simulations. In the simulation, the robot, obstacles and goal are assumed as unit masses, and the initial position of robot, obstacles and goal are fixed randomly. The speed of obstacles and goal are also random, and the initial speed of robot is zero.

To obtain the universality, 1,000 random simulation experiments for one set of k_1:k_2:k_3 were carried out, and the simulations using tAPF and iAPF are both carried out under the same conditions. By varying the weights by an interval of 1 per cent, we traverse all the values in (0,1), and ensure that $k_1 + k_2 + k_3 = 1$, i.e. we vary the k_1, k_2, k_3 to take the weights from 1 to 100 per cent. The results for four-wheeled OMR are shown in Figure 12. The results for the three-wheeled OMR can be shown in the same form, which are not listed here. The path length, average velocity, time consumption and energy consumption are analysed. In the Figure, every grid corresponds a set of k_1, k_2, k_3, and the colour of the grid records a percentage improvement of our iAPF over tAPF in the 1,000 simulations. Where, the x-axis is k_1, and y-axis is k_2.

With the simulation results (Figure 12), we can use them as a reference to obtain the motion plan that meets our pre-requisites. For example, for the soccer robot we set $k_1 = 70$ per cent, $k_2 = 30$ per cent, $k_3 = 0$ per cent, because speed of planning is weighed as more important than efficiency.

One of the simulation cases carried out on the four- and three-wheeled OMR are shown in Figure 13. In the cases, we set $k_1 = 50$ per cent, $k_2 = 25$ per cent, $k_3 = 25$ per cent. The results are also compared between tAPF and iAPF in Table II. From these data, we can conclude that the iAPF distinctly outweighs that of tAPF.

5.2 Experiment results

The occurrence of skids and other practical kinematic and dynamic constraints of the OMR are not considered in the simulation work. Therefore, we carried out some experiments to investigate the practical motion efficacy achieved using the improved motion planning method. Also the stability anisotropy will be validated in this section.

In the experiments, the home care robot (Figure 2(a)) and the middle-size soccer robot (Figure 2(b)) are used. They consist of four omni-directional wheels and three omni-directional wheels, respectively. The weight of the home care robot is about 30 kg, and the dimensions are $50 \times 50 \times 150$ mm. The weight of the soccer robot is about 20 kg, and the dimensions are $50 \times 50 \times 80$ mm.

The hardware of the motion control system of the two kinds of robot is almost the same. We use a laptop computer as a high-level controller for the behaviour-based control, and we use the Maxon motion controller (EPOS 24/5) to control the robot velocity depending on the feedback encoder data. The higher level controller and the motion controller are connected via CAN bus.

Table I Setup for simulation

P_4 (N)	P_3 (N)	R (m)	r (m)	J_d(kg m^2)	J_p(kg m^2)	M_{P_p}(N m)	M_{P_d}(N m)	k_a	k_b	k_0	u_h	n_1	n_2	$\|d_i\|$(m)	D_0(m)
294	196	0.04	0.015	0.5482×10^{-4}	5.675×10^{-3}	0.392	0.147	0.1	0.2	0.8	1.12	0.4	0.3	0.22	1

Note: SI units

Figure 12 A 1,000 random simulation results

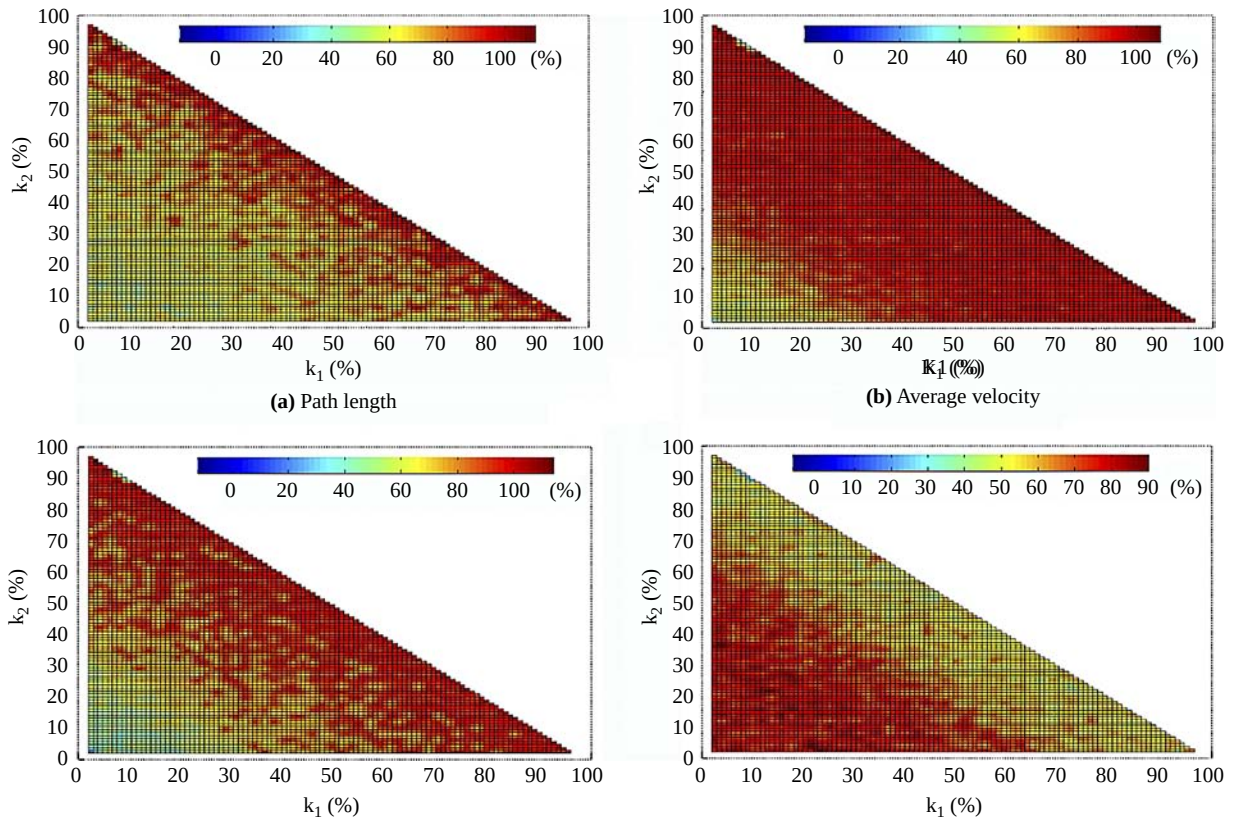

(a) Path length

(b) Average velocity

(c) Time consumption

(d) Energy consumption

Figure 13 Trajectories of four- and three-wheeled OMR

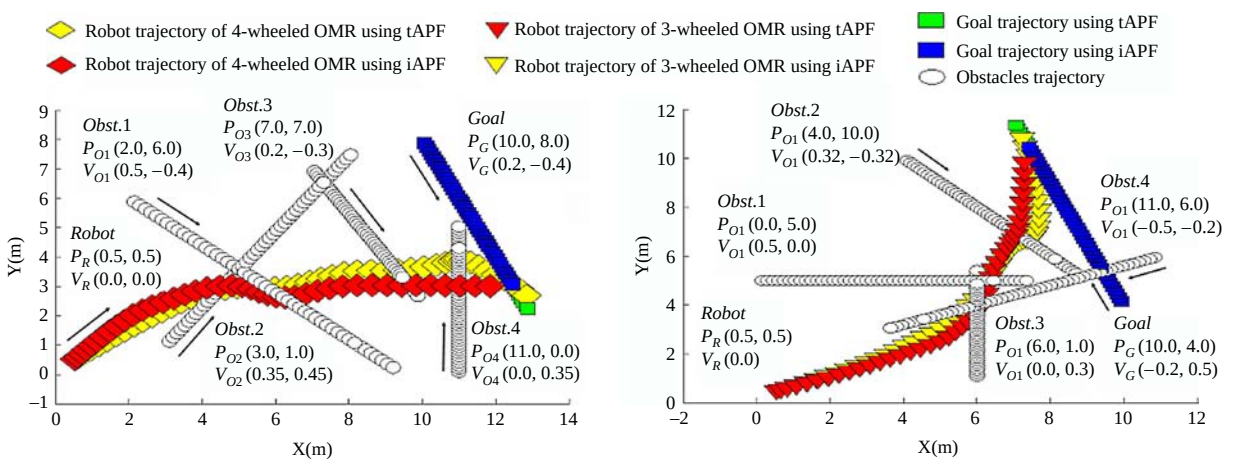

(a) Simulation carried out on four-wheeled OMR

(b) Simulation carried out on three-wheeled OMR

Table II Simulation results of four- and three-wheeled OMR

	Path length (m)		Energy consumption (kgf·m)		Average velocity (m/s)		Time consumption (s)	
	Four-wheeled	Three-wheeled	Four-wheeled	Three-wheeled	Four-wheeled	Three-wheeled	Four-wheeled	Three-wheeled
tAPF	13.69	14.21	592.82	641.95	0.94	0.96	14.53	14.95
iAPF	12.55	13.17	540.16	556.21	1.00	1.01	12.49	13.15

The motors used for the omni-directional robot are Maxon DC motors (RE36 series, 24v, 70w), and the gearheads are Maxon's planetary gearhead series GP32 A (Nominal reduction ratio 14:1). And the Maxon Photoelectric Encoder HEDL 5540 (pulse per resolution 512) is used for feedback in the robot.

The Wiimote (Figure 14), which serves as the wireless input for the Nintendo Wii gaming console, can detect motion and rotation in three dimensions through the use of accelerometer technology. In the experiments, each robot is attached with the Wiimote. We use the Wiimote's acceleration sensor independent of the gaming console for measuring the position of the robot.

The experiment is carried out on the green carpeted field for RoboCup middle size robot play (12×8 m), where we take a red box put on a robot as the goal, three black robots as the obstacles.

Owing to the high centre of gravity, it is easy for the robot to tip over with a high speed motion for the home care robot. The maximum speed of the four-wheeled OMR is set at 0.6 m/s. We take $k_1 = 20$ per cent, $k_2 = 80$ per cent, $k_3 = 0$ per cent for the four-wheeled OMR to achieve a highly stable motion plan, and take $k_1 = 70$ per cent, $k_2 = 30$ per cent, $k_3 = 0$ per cent for the three-wheeled OMR to achieve a high-speed motion plan. Owing to the difficulty of measuring the energy consumption, we did not consider this item by taking $k_3 = 0$ per cent in the experiments.

First, we let the goal move at an initial speed in the field. At the same time, the obstacles move at the set speed, and the omni-directional robots try to catch the goal while avoiding collision with the obstacles in two different motion planning methods, the tAPF and iAPF proposed above.

Figure 15(a) and (b) shows the experiment setup. The initial position and velocity of the robot, obstacles and goal of the experiment are set as shown in Figure 16, and the coordinates established, in which the centre of the robot is the origin, the front of the robot is y-axis.

As the experiment results, both of the four- and three-wheeled OMR can reach the goal successfully while avoiding the obstacles in the experiment, and the efficacy of the iAPF is better than that of the tAPF. The results of the experiment are shown in Figure 16 and Table III.

Figure 14 Wiimote

In Figure 16, the theoretic trajectories are derived from the motion planning simulated by Matlab with the initial setup in Table I, and the practical trajectories are the robot trajectories in the experiment. From the results shown in Figure 16, there are some obvious deviations between the theoretic value and experimental value, and the deviations are shown in Figure 17. And the reasons resulting in the deviations can be analysed as follows. First, although we tried the setup in Table I to approach a "real" case, there were also some deviations inevitably due to the uncertainty of the robot and the environment. Second, because of the characteristics of the omni-directional wheel, the robot tends to "skip" during motion, and the theoretical curves simulated by Matlab did not take the "skip" into account.

Based on the data in Figure 17, we can conclude that, there is less skip for the motion resulting from the iAPF than the one resulting from the tAPF to a certain extent. The deviations of the four-wheeled OMR are much less than that of three-wheeled OMR, which validates the motion stability item of the anisotropic function is very useful for the improved motion planning method.

6. Conclusion

By analysis of the driving torque acting on each wheel and the maximum acceleration of the OMR, the motion stability anisotropy is introduced into the anisotropic function. Also the velocity and the motion efficacy are discussed as the important indicator for motion planning. Considering the collision-free path and shorter path as the pre-requisites of the motion plan, we determined the VMDR. And according to the anisotropic function, we varied the motion direction in the VMDA to achieve better motion results. Using the simulation data, we could vary the weights of the anisotropic function to achieve the motion we need. Finally, with the right weights of the anisotropic function, an iAPF was proposed to exhibit the motion potential of OMRs. In order to validate the universality of the proposed motion planning method, the OMRs with different arrangements of wheels are discussed, such as three- and four-wheeled OMR. By carrying out experiments on real robots, the practicability of the anisotropic function is validated.

But the practical factors, such as the effect of wear on the omni-directional wheels, were not considered during the deduction. Therefore, in future research, it is necessary to take this issue into account to obtain a more accurate model for the anisotropic function. In this study, the main objective is to find a high-speed, highly stable and highly efficient motion plan suitable for OMRs. Typical problems of tAPF, e.g. local minimum problem, are not addressed here, which is beyond the scope of this study. In our future research we will deal with these issues.

Figure 15 Experiment scene with iAPF

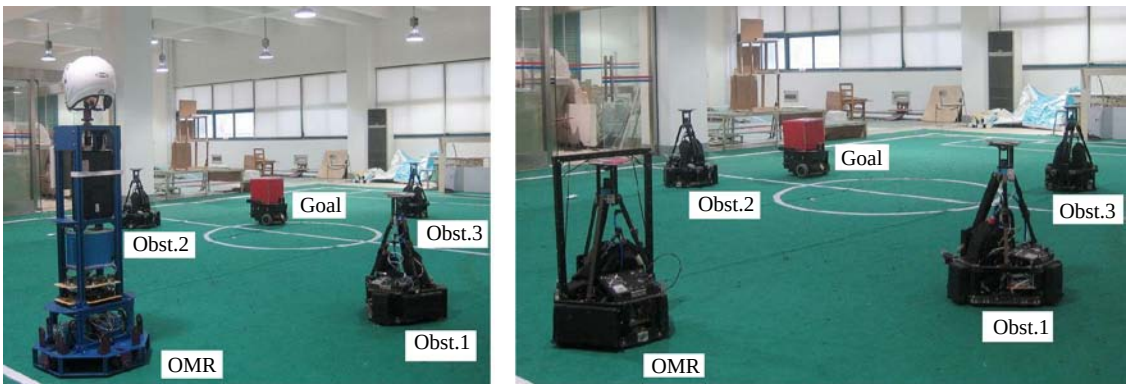

(a) Four-wheeled OMR **(b)** Three-wheeled OMR

Figure 16 The theoretic and practical trajectory

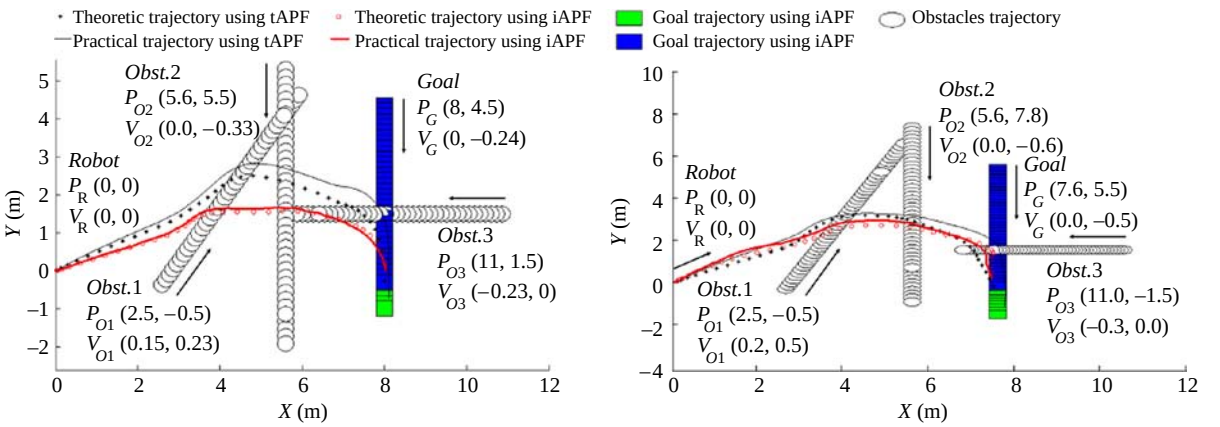

(a) Trajectory of four-wheeled OMR **(b)** Trajectory of three-wheeled OMR

Table III Result data of experiment

	Path length (m)		Average velocity (m/s)		Time consumption (s)	
	Four-wheeled	Three-wheeled	Four-wheeled	Three-wheeled	Four-wheeled	Three-wheeled
tAPF	10.54	12.15	0.45	0.85	23.24	14.29
iAPF	9.11	10.02	0.44	0.87	20.68	11.52

Figure 17 The deviations between the theoretic trajectory and the practical trajectory

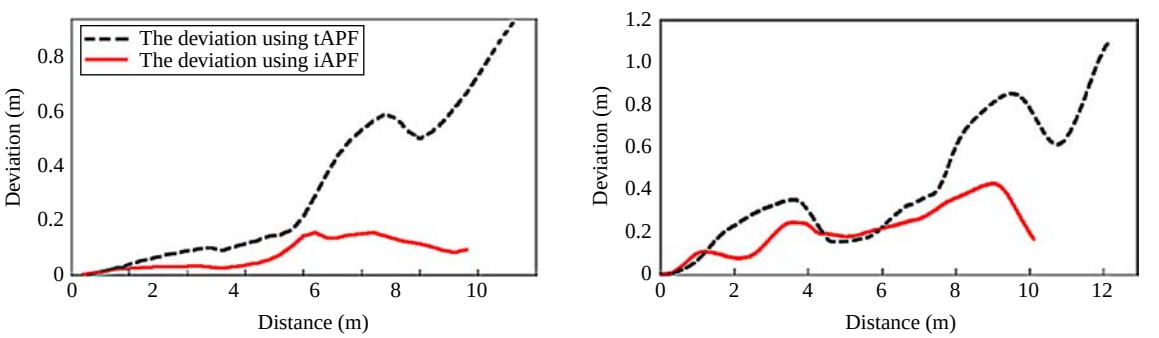

(a) Deviations for four-wheeled OMR **(b)** Deviations for three-wheeled OMR

References

Angeles, J. (2003), *Fundamentals of Robotic Mechanical Systems: Theory, Methods, and Algorithms*, 2nd ed., Springer, New York, NY.

Balkcom, D.J., Kavathekar, P.A. and Mason, M.T. (2006), "The time-optimal trajectories for an omni-directional vehicle", *International Journal of Robotics Research*, Vol. 25 No. 10, pp. 985-99.

Brock, O. and Khatib, O. (1999), "High-speed navigation using the global dynamic window approach", *Proceedings of IEEE Conference on Robotics and Automation, Piscataway, NJ*, pp. 341-6.

Chatzakos, P., Markopoulos, Y.P., Hrissagis, K. and Khalid, A. (2006), "On the development of a modular external-pipe crawling omni-directional mobile robot", *Industrial Robot: An International Journal*, Vol. 33 No. 4, pp. 291-7.

Felipe, H. and Miguel, T. (2006), "A comparison of path planning algorithms for omni-directional robots in dynamic environments", *IEEE 3rd Latin American, Robotics Symposium (LARS '06)*, October, pp. 18-25.

Ferriere, L., Raucent, B. and Campion, G. (1996), "Design of omnimobile robot wheels", *Proceedings of the IEEE International Conference on Robotics and Automation, Minneapolis, MN*, pp. 3664-70.

Ge, S.S. and Cui, Y.J. (2002), "Dynamic motion planning for mobile robots using potential field method", *Autonomous Robots*, Vol. 13 No. 3, pp. 207-22.

Jing, X.J., Wang, Y.C. and Tan, D.L. (2004), "Artificial coordinating field and its application to motion planning of robots in uncertain dynamic environments", *Science in China, Series E, Engineering & Materials Science*, Vol. 47 No. 5, pp. 577-94.

Kalmar-Nagy, T., D'Andrea, R. and Ganguly, P. (2004), "Near-optimal dynamic trajectory generation and control of an omnidirectional vehicle", *Robotics and Autonomous Systems*, Vol. 46 No. 1, pp. 47-64.

Khatib, O. (1986), "Real-time obstacle avoidance for manipulators and mobile robots", *International Journal of Robotics Research*, Vol. 5 No. 1, pp. 90-8.

Koh, K.C. and Cho, H.S. (1999), "A smooth path tracking algorithm for wheeled mobile robots with dynamic constraints", *Journal of Intelligent and Robotic Systems*, Vol. 24 No. 4, pp. 367-85.

Leng, C.T. and Cao, Q.X. (2006), "Velocity analysis of omnidirectional mobile robot and system implementation", *IEEE International Conference on Automation Science and Engineering, Shanghai*, pp. 81-6.

Luh, G.C. and Liu, W.W. (2007), "Motion planning for mobile robots in dynamic environments using a potential field immune network", *Proceedings of the Institution of Mechanical Engineers, Part I: Journal of Systems and Control Engineering*, Vol. 221 No. 7, pp. 1033-46.

Pin, F.G. and Killough, S.M. (1994), "A new family of omni-directional and holonomic wheeled platforms for mobile robots", *IEEE Transactions on Robotics and Automation*, Vol. 10 No. 4, pp. 480-9.

Samani, A.H., Abdollahi, A., Ostadi, H. and Rad, S.Z. (2004), "Design and development of a comprehensive omni directional soccer player robot", *International Journal of Advanced Robotic Systems*, Vol. 1 No. 3, pp. 191-200.

Shimoda, S., Kuroda, Y. and Iagnemma, K. (2005), "Potential field navigation of high speed unmanned ground vehicles on uneven terrain", *IEEE International Conference on Robotics and Automation, Barcelona*, pp. 2828-33.

Suzuki, T. and Shin, S. (2005), "Goal-directed navigation strategy for a mobile robot under uncertain world knowledge", *Proceedings of the IEEE International Conference on Mechatronics and Automation, Canada*, pp. 741-6.

Tlale, N.S. (2006), "On distributed mechatronics controller for omni-directional autonomous guided vehicles", *Industrial Robot: An International Journal*, Vol. 33 No. 4, pp. 278-84.

Wang, S.M., Lai, L.C., Wu, C.J. and Shiue, Y.L. (2007), "Kinematic control of omni-directional robots for time-optimal movement between two configurations", *Journal of Intelligent and Robotic Systems*, Vol. 49 No. 4, pp. 397-410.

Wu, J. (2004), "Dynamic path planning of an omni-directional robot in a dynamic environment", PhD dissertation, Ohio University, Athens, OH.

Wu, J., Williams, R.L. II and Lew, J. (2006), "Velocity and acceleration cones for kinematic and dynamic constraints on omni-directional mobile robots", *Journal of Dynamic Systems, Measurement, and Control*, Vol. 128 No. 4, pp. 788-99.

Yu, Z.S. (1990), *Automoblie Theory*, China Machine, Beijing.

Zheng, T.X. and Zhao, X.Y. (2006), "A novel approach for multiple mobile robot path planning in dynamic unknown environment", *IEEE International Conference on Cybernetics & Intelligent System (CIS) and Robotics, Automation & Mechatronics (RAM), Bangkok*, pp. 46-50.

Corresponding author

Chuntao Leng can be contacted at: ctleng@sjtu.edu.cn